Effects of interfacial depletion on the degradation of SiAlN coating

Zhaohe Gao[a,b*], Justyna Kulczyk-Malecka[c], Peter Kelly[c] and Ping Xiao[a*]

[a]*Henry Royce Institute, Department of Materials, University of Manchester, Manchester, M13 9PL, UK*
[b]School of Metallurgy & Materials, University of Birmingham, Birmingham, B15 2TT, UK
[c]*Surface Engineering Group, Manchester Metropolitan University, Manchester, M1 5GD, UK*

Abstract

Thermally stable 0.4 μm, 0.8 μm, and 1.6 μm thick SiAlN coatings with Mo interlayers have been deposited on Ti substrates to serve as a protective barrier layer for aeroengine applications. After 50 h (10 cycles) of exposure at 800°C in air, the 0.4 μm, 0.8 μm thick SiAlN coatings were depleted to tens of nanometers in thickness and then formed oxide scales, whereas 1.6 μm thick SiAlN coating retained a 0.5 μm thick remnant SiAlN layer without any observable oxidation. The depletion of the SiAlN coating is induced by purely interfacial diffusion/reactions with the underlying substrate. Once depleted to a few tens of nanometers thick, i.e., close to being fully depleted, the SiAlN coating starts to oxidise, along with an elemental composition change in the remnant SiAlN. The degradation mechanism of the SiAlN coating is determined by its depletion, as opposed to the interfacial reaction induced microstructural change of the remnant coating.

Keywords: Depletion; SiAlN coating; Oxidation; Degradation; Interfacial reaction.

1. Introduction

Innovative technology and innovative design concepts for fuel-efficient and hybrid-electric airplanes or automobiles are critical in order to move to a low carbon economy to mitigate climate change, and for our prosperity, health, and our future [1, 2]. Such fuel-efficient innovations have increasingly been exploring lightweight structural materials, e.g. Ti alloys (high strength-to-weight), and also exposing such structural alloys (e.g. Ti6Al4V and Ti6246 for blades, or turbochargers) to high temperature and chemically aggressive, demanding environments [3-11]. However, Ti alloys have inadequate oxidation resistance upon high temperature exposure due to the less protective native oxide scale that forms, especially at temperatures above 500°C [12]. Therefore, the use of Ti alloys will rely on novel coating solutions to provide improved oxidation resistance of Ti alloys in such demanding environments [12]. The advantage of designing protective coatings against oxidation include cost effectiveness; in

z.gao.1@bham.ac.uk (Z.G.) p.xiao@manchester.ac.uk(P.X.)

providing good oxidation resistant coating materials and good interfacial performance without significantly increasing component weight [13]. There are considerable numbers of oxidation resistant materials that could fulfil the requirements, including aluminide and silicide coatings that form protective oxide films at the surface, and thermal stable ceramic coatings, e.g. glass-ceramic, nitrides (TiAlN, SiAlN) [13-22]. Nevertheless, both the metallic coatings (aluminide/silicide) and ceramic coatings could undergo premature failure due to their poor interfacial performance. The interdiffusion or inter-reaction between coatings and the underlying substrates (e.g. Ti alloy) can inevitably occur due to their chemical incompatibility, resulting in the depletion of coatings and/or degradation of the interfacial mechanical performance due to the formation of brittle phases at the coating/substrate interface [13, 23-28]. In contrast, our previous work has taken advantage of modifying the interdiffusion/interaction zone between SiAlN nitride coatings and the underlying Ti substrate via inserting a Mo interlayer. The interaction between SiAlN and Ti enables the formation of a new interlayer exhibiting adaptive conformability via mechanical twinning within the interfacial product. The interdiffusion between Mo and Ti avoids the formation of a brittle phase at the interface, thereby providing good interfacial performance [13]. However, the beneficial interfacial reaction continuously consumes the SiAlN coating during thermal exposure, thus, the SiAlN coating must not be fully depleted as the remnant SiAlN coating is the outermost protective layer against oxidation. Therefore, whether there is a critical thickness for the as-deposited SiAlN coating, and how the interfacial reaction affects the microstructure/composition of remnant SiAlN coatings, and how the interfacial depletion affects the degradation of SiAlN, need to be uncovered. Also, the effect of the Mo interlayer on the formation and distribution of twinning in the interfacial product remains unclear.

In this study, we have deposited 0.4 µm, 0.8 µm, and 1.6 µm thick SiAlN coatings, with or without a 0.3 µm Mo interlayer on Ti substrates by magnetron sputtering. After identical thermal exposure, the oxidation and degradation mechanisms of the SiAlN/Mo coatings with different thicknesses have been studied. The effect of interfacial reaction on the oxidation and degradation of the SiAlN coatings and the effects of Mo on the formation of a twining interlayer have also been examined.

2. Experiments and methods

2.1 Sample preparation

The SiAlN coatings of different thicknesses with or without Mo interlayers were deposited on one side of pure Ti coupons (30 × 30 × 2 mm^3) in a Teer Coatings Ltd. UDP 350 magnetron sputtering system.

The Ti coupons were ground, polished, and ultrasonically cleaned prior to deposition. The 99.95% pure Si, Al, and Mo targets (300 x 100 mm^2) were fitted onto unbalanced magnetrons and installed through the chamber walls, surrounding a centrally mounted, rotating, unheated substrate holder. The polished substrates were bias cleaned in Ar+ ions by applying a DC bias of -600 V for 15 minutes. The Mo interlayer was then deposited in an Ar-only environment. The Mo target was driven by a pulsed DC power supply (Advanced Energy Pinnacle Plus) at a power of 500 W and 100 KHz frequency (50% duty). Following the Mo interlayer deposition, the SiAlN coating was deposited in an Ar and N_2 atmosphere, and the Si and Al targets were powered at 700 W and 300 W, respectively. The Ar and N_2 gas ratio during coating deposition were controlled by a mass flow controller and the partial pressure of the chamber was also monitored, details reported in our previous work [13]. A bias of -30 V was applied to the substrate throughout the Mo and SiAlN coating deposition and the substrate holder was rotated at a speed of 5 rpm. The different thicknesses of Mo and SiAlN coatings were controlled by the deposition duration.

The coated coupons were cut into smaller rectangular pieces (10 × 10 × 2 mm^3) using a SiC abrasive cutting blade and the smaller pieces used for oxidation tests were cleaned with soapy water and acetone. The SiAlN coated Ti samples, with or without Mo interlayers, were thermal tested at 800°C for 5 h in air in a CM™ furnace with a heating rate of 100°C/ minute and followed by forced air cooling for 10 minutes (sample stage out of the heating zone), then returned for the next cycle.

2.2 Characterisation

The top surfaces and cross-sections of as-deposited and oxidised SiAlN/Mo coated samples were investigated by scanning electron microscopy (SEM, FEI, Quanta 650, and Magellan HR), coupled with a focused ion beam (FEI, Helios 660). To investigate the microstructure and composition of the as-deposited and oxidised coatings in greater detail, thin lamellae had been prepared by FIB via a lift-out technique and then investigated by transmission electron microscopy (TEM, FEI, Talos F200A) fitted with Super - X- EDS system. The composition depth profiles of as-deposited and oxidised coatings were also studied by focused ion beam – X-ray photoelectron spectroscopy (FIB-XPS, Kratos AXIS Supra) and the depth was measured and validated, as described in detail elsewhere [23].

3. Results

3.1 As-deposited SiAlN/Mo coatings

Fig.1 shows cross-sectional SEM micrographs of as-deposited SIAlN and SiAlN/Mo coatings with different thicknesses, i.e. 0.8 µm thick SiAlN coating without Mo interlayer (Fig.1 a), 0.4 µm thick SiAlN coating with 0.3 µm thick Mo (Fig.1 b), 0.8 µm thick SiAlN coating with 0.3 µm thick Mo (Fig.1 c), 1.6 µm thick SiAlN coating with 0.3 µm thick Mo (Fig.1 d). The 0.3 µm thick Mo interlayer, deposited between the Ti substrate and SiAlN, plays a bonding role between the substrate and nitride coating. The SiAlN coatings show smooth, glass-like homogeneous microstructures without any observable cracks or pores. And the SiAlN coatings are fully dense without any sign of defects having been deposited under identical conditions and parameters. The SiAlN coatings display an amorphous microstructure and consist of amorphous AlN and Si_3N_4 phases, where AlN nanoparticles are uniformly dispersed in the Si_3N_4 matrix, which is well reported by our previous work [13].

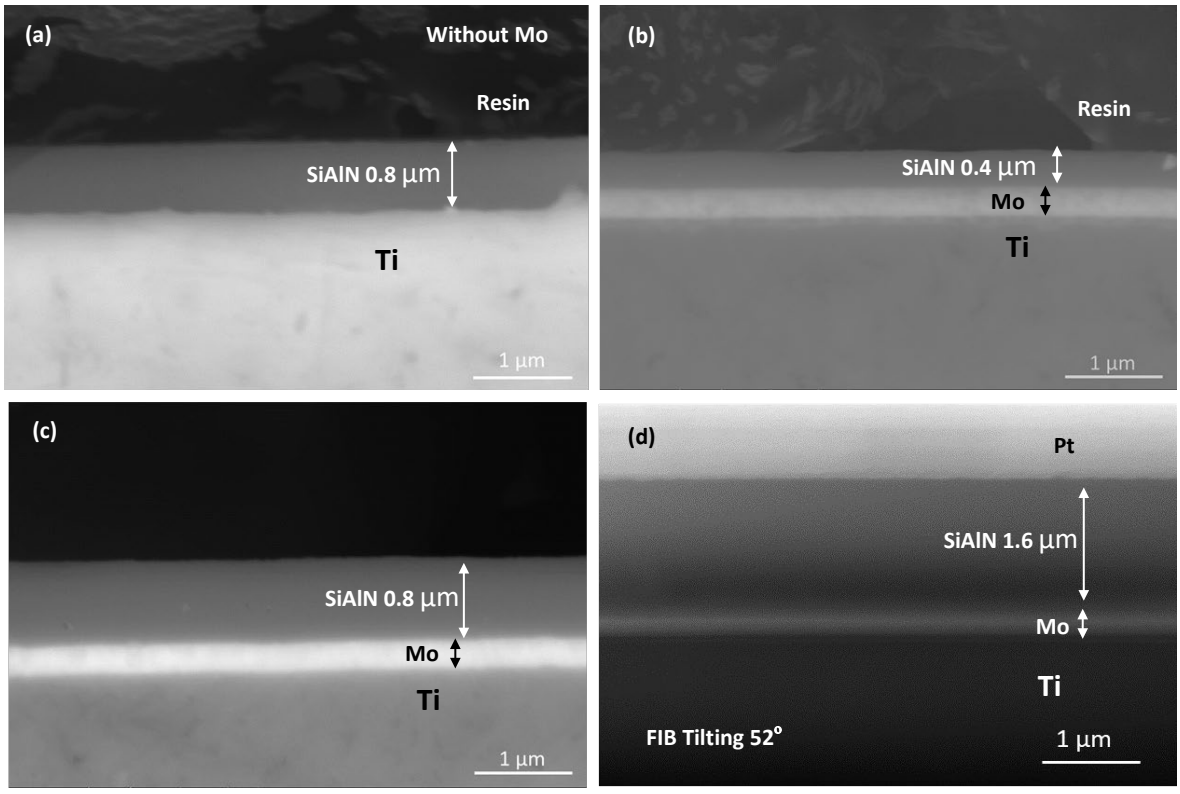

Fig.1 Cross-sectional SEM micrographs of as-deposited SiAlN/Mo coatings in different thickness: (a) SiAlN (0.8 µm thick) without Mo, (b) SiAlN (0.4 µm thick) with Mo (0.3 µm), (c) SiAlN (0.8 µm thick) with Mo (0.3 µm), (d) SiAlN (1.6 µm thick) with Mo (0.3 µm).

3.2 Oxidation behaviour in relation to SiAlN coating thickness

Fig. 2 shows cross-sectional SEM micrographs and top surface SEM images of SiAlN/Mo coatings with different thicknesses after oxidation at 800°C in the air for 20 h (4 cycles). It is obvious that the SiAlN coating without a Mo interlayer (Fig.2 a1) has cracked upon 4 cycles of oxidation, whereas the SiAlN coatings with Mo interlayers (Fig.2 b1-c1) show no sign of cracking on the top surface of the coating. Moreover, coating stacks with an identical 0.3 µm thick Mo interlayer, but different SiAlN coating thicknesses of 0.4 µm (Fig. 2 b/b1), 0.8 µm (Fig.2 c/c1), 1.6 µm (Fig.2 d/d1), respectively, display different oxidation behaviours, ranging from the formation of thick oxide scale (Fig. 2 b1), to a few localised oxidation spots (Fig. 2 c1), to no observable oxidation (Fig. 2 d/d1) after 20 h thermal exposure. It can also be observed that there is interdiffusion between the Mo interlayer and underlying Ti, forming a Ti-Mo solid solution diffusion zone. Also, the inter-reaction between SiAlN and Ti causes the formation of a new interlayer consisting of $TiN_{0.26}$ and Ti_5Si_3, and this phenomenon will be discussed in detail later.

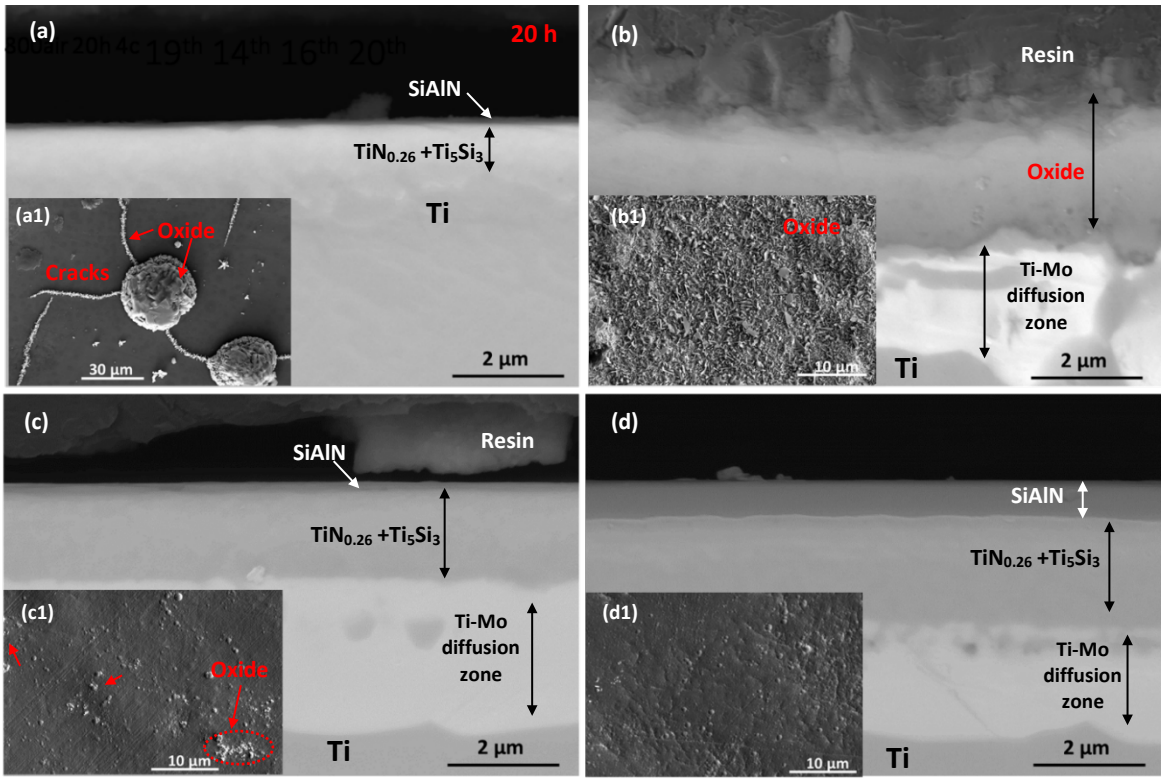

Fig.2 Cross-sectional SEM micrographs and top surface SEM images of SiAlN/Mo coatings after oxidation at 800°C for 20 h (4 cycles): (a) SiAlN (0.8 µm thick) without Mo, (b) SiAlN (0.4 µm thick) with Mo (0.3 µm), (c) SiAlN (0.8 µm thick) with Mo (0.3 µm), (d) SiAlN (1.6 µm thick) with Mo (0.3 µm).

In order to investigate how SiAlN/Mo coatings degrade, the 0.4 µm thick SiAlN coating with a 0.3 µm thick Mo layer was exposed to a relatively short thermal cycle duration of 5 h (1 cycle) at 800°C. Fig. 3 shows the top surface and cross-sectional micrographs of SiAlN (0.4 µm thick) with Mo (0.3 µm) after oxidation at 800°C for 5 h (1 cycle). As can be seen in Fig. 3 a, the top surface of the SiAlN coating has a considerable number of oxide nucleation sites. To view this in finer detail, thin lamellas of the cross-section of the coating, covering the flat zone 'B' and oxide nucleation location 'C' in Fig.3 a, were prepared by FIB using the lift-out technique and then analysed by STEM/EDS, as shown in Fig.3 b and c, and Fig.S1 in Supplementary Material. The HAADF micrographs along with the corresponding EDS mappings (Fig. 3 b and c), display that there is a great deal of inter-reaction between the SiAlN coating and underlying Ti.

During thermal exposure, the Ti reacts with Si_3N_4 and AlN (SiAlN is a mixture of Si_3N_4 and AlN), forming $TiN_{0.26}$ and Ti_5Si_3, marked in Fig. 3 b/c, as shown in equations 1, 2, and 3, also confirmed by our previous work [13]. Noticeably, the as-deposited 0.4 µm thick SiAlN has been reduced to tens of nanometres in thickness in places due to above mentioned inter-reaction or was fully consumed, as shown in Fig. 3 b and c, respectively. The residual SiAlN coating, the 'flat zone B' in Fig. 3 a, also oxidises and forms a thin layer of oxide consisting of SiO_2 and Al_2O_3, also illustrated by XPS analysis (Fig.11) below. In the oxide nucleation location, the SiAlN coating has been fully consumed and the bump oxide nucleation consists of a top TiO_2 layer and underlying SiO_2/Al_2O_3 mixture layer, as shown in Fig. 3 a and c.

$$Ti + 0.065Si_3N_4 = 0.195Si + TiN_{0.26} \qquad \Delta G(1073.15K) = -1.825\times10^4\ J/mol \qquad (1)$$

$$5Ti + 3Si = Ti_5Si_3 \qquad \Delta G(1073.15K) = -8.16\times10^5 J/mol \qquad (2)$$

$$Ti + AlN \longrightarrow Ti_{1-x}Al_x + TiN_{0.26} \qquad \Delta G(1073.15K, X=0.15,\ 0.15\ \text{max solid solution}) = -2.93\times10^3 J/mol \qquad (3)$$

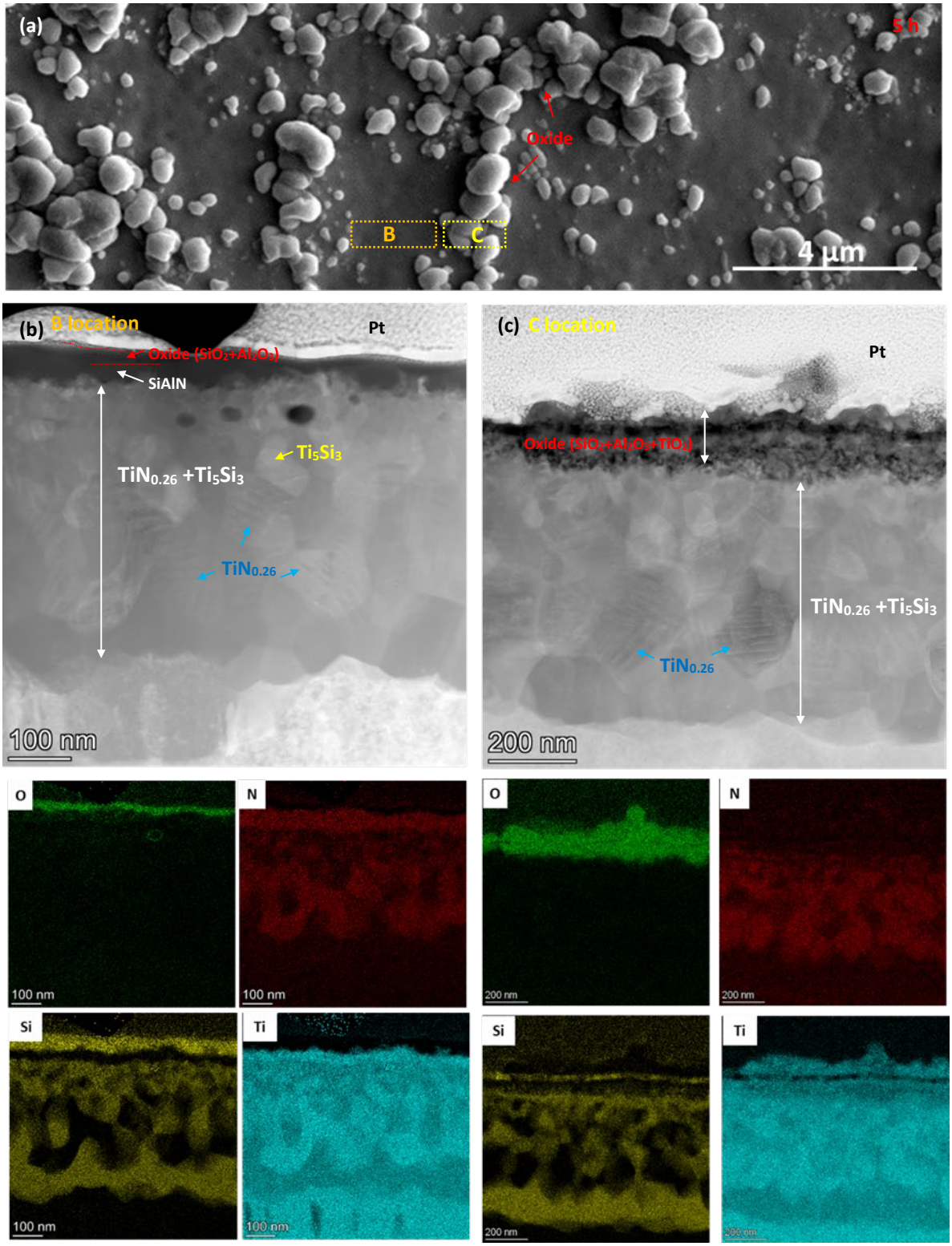

Fig.3 Top surface and cross-sectional micrographs of SiAlN (0.4 µm thick) with Mo interlayer (0.3 µm) after oxidation at 800°C for 5 h (1 cycle): (a) Top SEM surface, (b) Cross-sectional HAADF micrograph and corresponding EDS mappings (orange box in (a)), (c) Cross-sectional HAADF micrograph and corresponding EDS mappings (yellow box in (a)).

Fig.4 displays the cross-sectional HAADF image and corresponding EDS mappings of a 1.6 µm thick SiAlN coating with 0.3 µm Mo layer after oxidation at 800°C for 20 h (4 cycles). The same interdiffusion and inter-reaction rules apply to the thicker SiAlN coating after thermal exposure as they do in the 0.4 µm thick SiAlN case. However, it is obvious that there is no observable oxide scale on the top of the remnant SiAlN coating after oxidation for 20 h. It can be predicted that the SiAlN coating has excellent thermal stability without oxidation as long as the leftover SiAlN coating could survive the inter-reaction with the Ti substrate. The remnant SiAlN coating remains amorphous and its elemental compositions across the SiAlN coating also remain consistent without obvious gradient, as confirmed by Fig. 5.

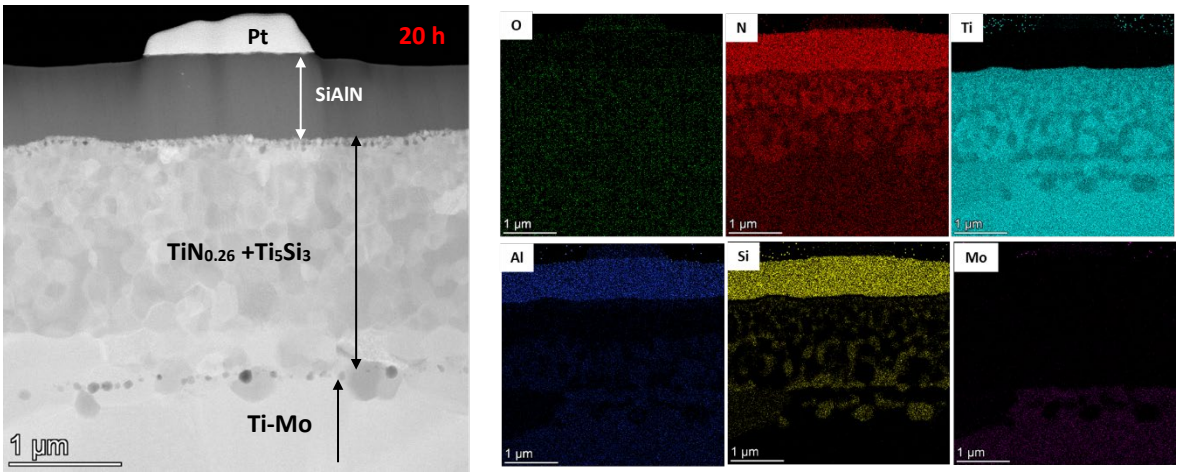

Fig.4 Cross-sectional HAADF micrograph and corresponding EDS mappings of SiAlN (1.6 µm thick) with Mo (0.3 µm) after oxidation at 800°C for 20 h (4 cycles).

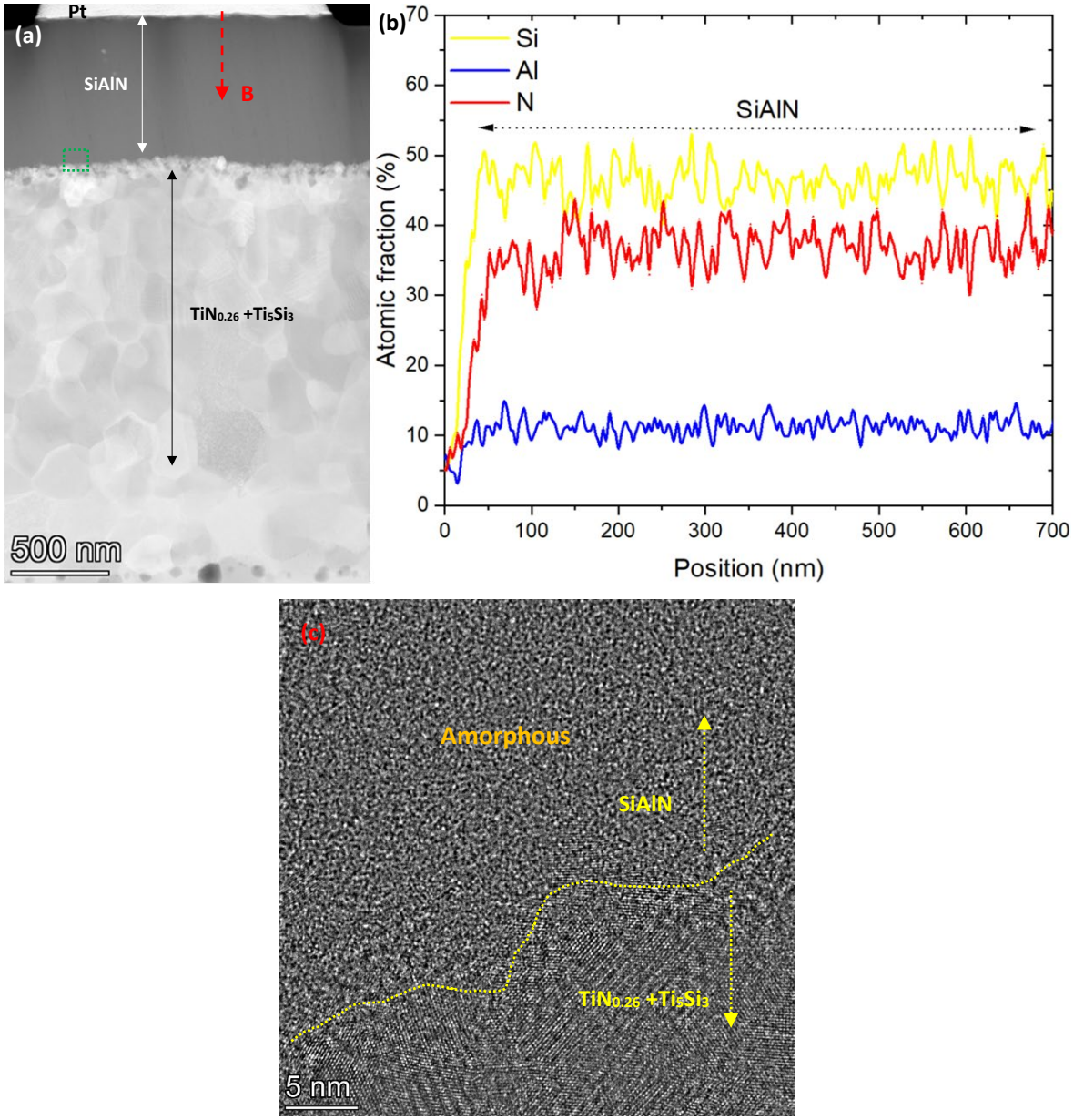

Fig.5 Cross-sectional HAADF/HRTEM micrographs and EDS line scans of SiAlN (1.6 µm thick) with Mo (0.3 µm) after oxidation at 800°C for 20 h (4 cycles): (a) HAADF image; (b) EDS line scan along the red line 'B' in (a); (c) HRTEM micrograph, from the framed green region in (a).

In order to verify the durability of the SiAN/Mo coating stack, the SiAlN coatings having different thicknesses of 0.4 µm, 0.8 µm, and 1.6 µm with 0.3 µm thick Mo interlayers were thermally cycled for 50 h (10 cycles) at 800°C and Fig. 6 a-c show the performance of the various SiAlN coatings (0.4 µm, 0.8 µm, and 1.6 µm thicknesses, respectively). It can be seen that a 4.3 um thick oxide scale has formed on the thinnest SiAlN coating case, see Fig.6 a, and a 3.3 um thick oxide scale has formed on the 0.8 µm thick SiAlN case in Fig. 6 b. However, there is no observable oxide scale on the thickest SiAlN

coating case, as shown in Fig.6 c. Noticeably, both oxide scales (consisting of TiO_2, SiO_2, and Al_2O_3) formed on the 0.4 µm and 0.8 µm SiAlN coatings show dense microstructure except cracking induced by thermal mismatch for the oxide scale formed on the 0.4 µm thick SiAlN case. Such dense oxide scales with a relatively low oxygen permeability could mitigate the oxidation of the underlying Ti, in comparison with about a 70 µm thick oxide scale formed on bare Ti after oxidation at 800°C for 50 h (10 cycles).

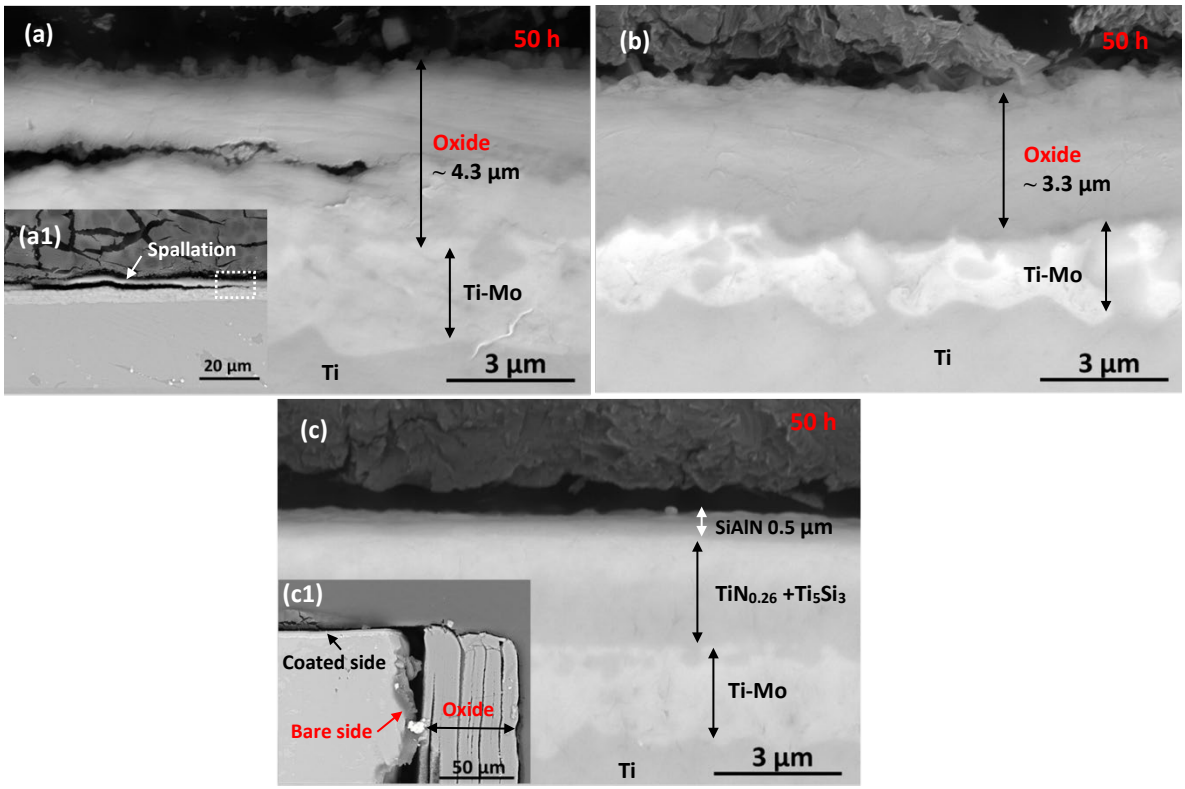

Fig.6 Cross-sectional SEM micrographs of SiAlN/Mo coatings after oxidation at 800°C for 50 h (10 cycles): (a) SiAlN (0.4 µm thick) with Mo (0.3 µm), insect (a1) showing the lower magnification, (a) is enlarged image from rectangle box in (a1); (b) SiAlN (0.8 µm thick) with Mo (0.3 µm); (c) SiAlN (1.6 µm thick) with Mo (0.3 µm), insect (c1) showing the coated side and bare Ti side.

3.3 Interfacial reaction zone in relation to Mo

It has been observed that the SiAlN coating without a Mo interlayer cracks upon thermal cycling, whereas no visible sign of cracking could be seen in the SiAlN coatings with Mo interlayers (Fig.2 a1-d1). The coating system integrity, e.g. no cracking and no spallation, could be influenced by the coating/substrate adhesion and thermal mismatch between coating and substrate upon thermal cyclic exposure. Fig.7 shows cross-sectional HAADF micrographs and corresponding EDS mappings of SiAlN coatings with or without Mo interlayers after oxidation at 800°C for 20 h. Noticeably, the interfacial

zone for SiAlN coatings without Mo after 20 h thermal exposure is about 1 µm thick while the interfacial zone for SiAlN coatings with Mo is about 2 µm, confirmed by Fig.7 a and b, respectively. Due to the high diffusivity of Mo in Ti (2.3×10^{-14} cm^2/sec, at 800°C) and the complete solubility of Mo in Ti [29, 30], the Ti-Mo diffusion zone can rapidly form, thereby enhancing the adhesion of SiAlN coatings on substrates via the formation of chemical bonding for cases with Mo interlayers [13]. Moreover, the rapidly formed Ti-Mo solid solution allows the Ti to react with the adjacent SiAlN, as shown in equations 1 - 3. During the Ti/Si_3N_4 reaction, discontinuous Ti_5Si_3 phases are formed and mainly distributed between the $TiN_{0.26}$ layer and Ti-Mo layer. More importantly, the Si partly diffuses into the Ti-Mo solid solution and thereby reacts with Ti, resulting in the discontinuous distribution of intermetallic Ti_5Si_3 phases in the Ti-Mo solid solution layer. This, in turn, explains the formation of a continuous $TiN_{0.26}$ interlayer, as shown in Fig.8 schematic diagrams. The continuous $TiN_{0.26}$ interlayer via mechanical twinning and stacking faults had been reported to effectively accommodate the thermal mismatch strain between the SiAlN coating and underlying Ti substrate [13]. For the SiAlN coating without a Mo interlayer case, the $TiN_{0.26}$ grains consisting of deformation twins are discontinuous and have been segmented by the connected intermetallic compound Ti_5Si_3 grains, which is confirmed by the HAADF and corresponding Si and N EDS maps in Fig.7 b. It can be expected that the non-continuous twinning $TiN_{0.26}$ interlayer for the case of the SiAlN coating without a Mo interlayer could weaken the accommodation of the thermal mismatch strain between coating layers and Ti substrate in comparison to the continuous twining $TiN_{0.26}$ layer that has been formed in the SiAlN coatings with a Mo interlayer, as shown in Fig.7 and illustrated in Fig.8. Thus, the diffusion bonding and mitigation of thermal mismatch with the presence of Mo interlayer could explain the cracking of SiAlN coating without Mo case, as illustrated in Fig.8.

With Mo

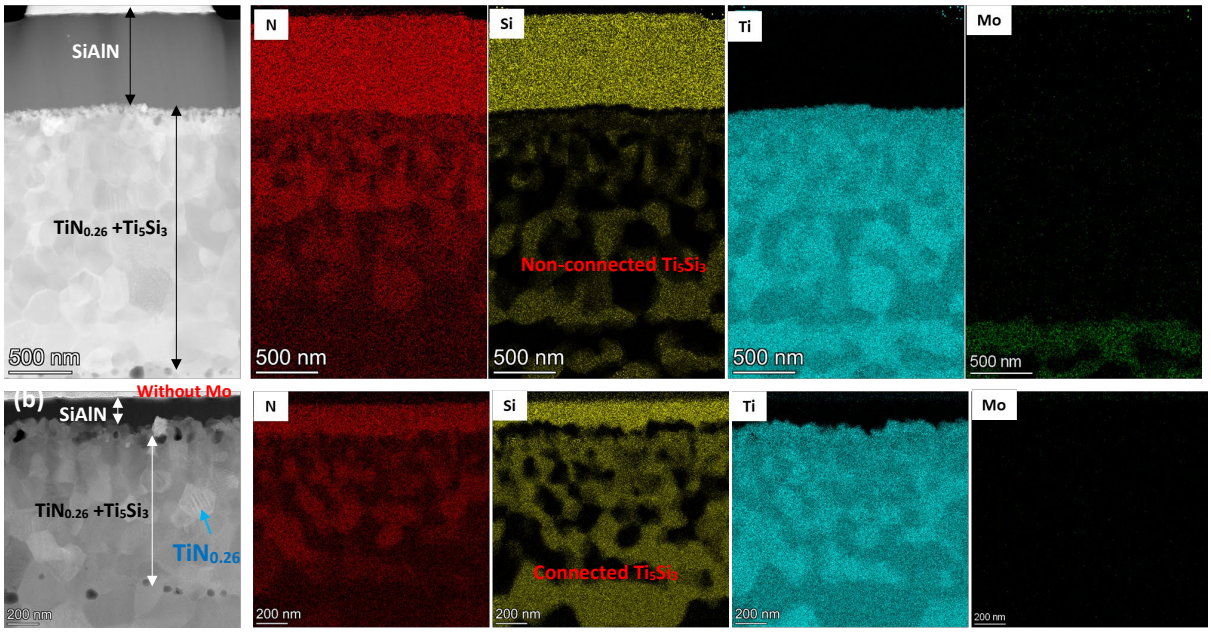

Fig.7 Cross-sectional HAADF micrographs and corresponding EDS mappings of SiAlN coating with or without Mo after oxidation at 800°C for 20 h: (a) SiAlN (1.6 μm thick) coating with Mo (0.3 μm), (b) SiAlN (0.8 μm thick) coating without Mo.

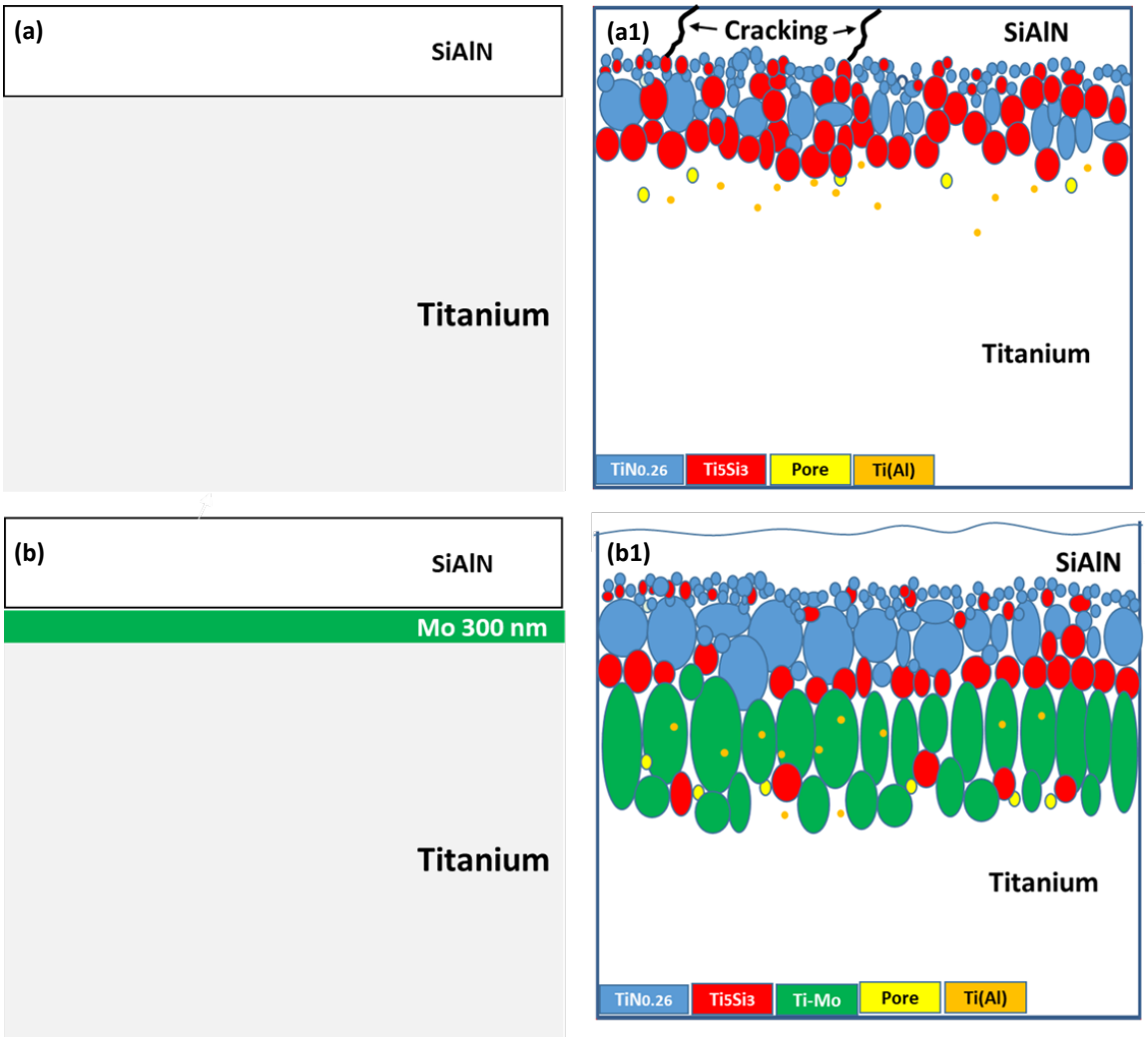

Fig.8 Schematic diagrams on the twinning distribution of SiAlN coatings with or without Mo interlayer after thermal exposure: (a) As-deposited SiAlN coating without Mo, (a1) Non-continuous $TiN_{0.26}$ twinning layer of SiAlN without Mo after thermal exposure, (a1) showing the existence of cracks after thermal exposure; (b) As-deposited SiAlN coating with Mo, (b1) Continuous $TiN_{0.26}$ twinning layer of SiAlN with Mo after thermal exposure.

4. Discussion

4.1 Degradation mechanism of amorphous SiAlN coatings

Previous studies have shown that amorphous SiMeN (Si_3N_4/MeN, Me=Al, Ti, Zr, Cr) coatings displayed good thermal stability and excellent oxidation resistance in oxidising species environments at high temperatures due to its high activation energy and extremely low parabolic rate constant of oxidation [23, 31-35]. Even though the amorphous SiMeN displays good intrinsic thermal stability, the

interdiffusion/inter-reaction between the underlying substrate could alter the microstructure and chemical composition of the top amorphous SiMeN coating. The degradation of amorphous SiMeN coatings mainly consists of two widely reported scenarios and one new scenario reported here: Ⅰ) interdiffusion induced crystallisation of the amorphous coating, Ⅱ) downward diffusion induced gradient composition across the coating, Ⅲ) interfacial reaction induced depletion of the coating, as shown by schematic diagrams in Fig.9. For scenario Ⅰ, numerous studies have shown that the elemental diffusion from the substrate into amorphous SiMeN coatings, and vice versa, could stimulate the crystallization of the amorphous coating, in turn, causing oxidation via grain boundary diffusion, a fast oxidation pathway in crystalline material [31, 36-38]. However, scenario Ⅰ lack detailed evidence on whether the amorphous coating undergoes crystallisation, thereby remaining unclear to a certain extent. For scenario Ⅱ, it was proposed and reported in our previous work, that the downward diffusion of Si and N from amorphous SiAlN into the underlying Zr alloy in high temperature steam environments caused the compositional change in the remnant amorphous SiAlN coating, instead of promoting crystallisation, thereby causing the oxidation of the coating [23].

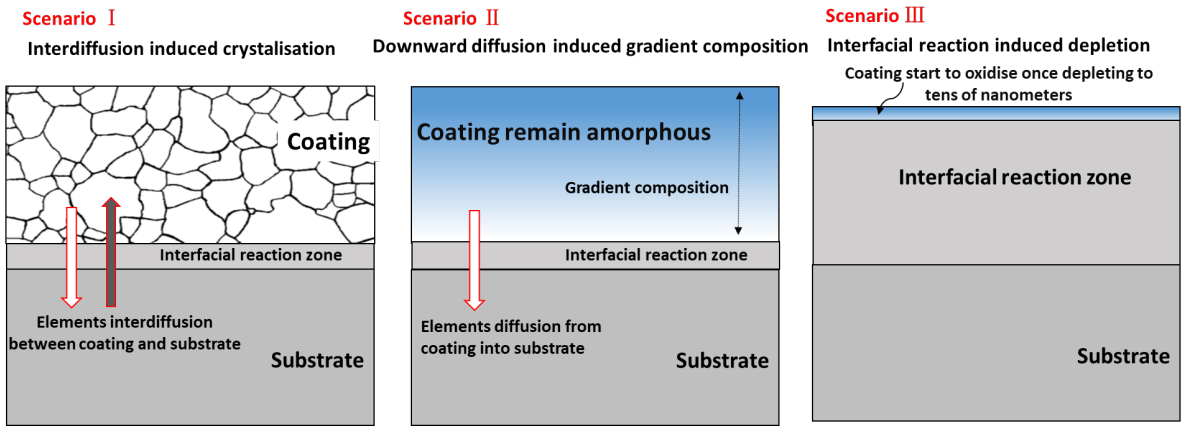

Fig.9 Schematic diagrams on degradation mechanism of amorphous nitride coatings in relation to interfacial diffusion/reaction.

This study neither supports the interdiffusion induced crystallisation of amorphous coating (scenario Ⅰ) nor follows the downward diffusion induced gradient composition across the coating (scenario Ⅱ). For the SiAlN/Mo on Ti case, the interdiffusion/inter-reaction causes the interfacial depletion of the SiAlN coating, without causing any upward diffusion of Ti into the SiAlN coating and downward diffusion of Si or N into the underlying Ti substrate, nor the crystallisation of remnant SiAlN, which can be confirmed by Figs. 3, 4, and 5. The SiAlN coatings are primarily consumed through interfacial inter-reaction with the underlying Ti. Once the remnant SiAlN coating is below a few tens of nanometres,

i.e., close to being fully depleted, as shown in Fig. 10 a-d, the interfacial reaction causes a chemical change in the composition of the remnant amorphous SiAlN coating, relative lower N content (< 30 at %) and higher Si (~50 at %), in comparison with the as-deposited SiAlN (N: > 40 at%). The SiAlN coatings with relatively lower N content tend to form the Si phase upon thermal exposure, confirmed by the FIB-XPS analysis on observation of Si_{2p}-Si_{2p} bonds in Fig.11 c. The Si has relatively lower activation energy upon thermal exposure and a higher parabolic rate constant of oxidation, in comparison with Si_3N_4 in the as-deposited SiAlN condition [23, 39, 40]. Thus, a thin oxide scale of tens of nanometres thickness has been formed on the remnant amorphous SiAlN coating confirmed by Fig. 10 b and c. This can be further supported by the fact the thickest SiAlN coating, 1.6 µm, does not display any observable oxide scale after thermal exposure for 20 h or even 50 h and the remnant amorphous SiAlN coating remains a few hundreds of nanometres thick and in its elemental composition, close to the as-deposited condition, as confirmed in Fig. 5 and Fig.6 c. Therefore, the degradation of the SiAlN coating is controlled by its depletion, as shown by Scenario ||| in Fig.9. The SiAlN coating deposited on Zr follows the degradation mechanism 'downward diffusion induced gradient composition across the coating (Scenario ||)', as shown in our previous work [23], whereas an identical SiAlN coating deposited on Ti follows the degradation mechanism described in Scenario |||. The reason for the abovementioned could be ascribed to N from SiAlN that does not combine with underlying Zr in the case of the Zr alloy and diffuses downwards far away from the interface, thereby causing substantial loss of N in the remnant SiAlN coating [23]. In contrast, in the case of Ti, N reacts with underlying Ti substrate forming $TiN_{0.26}$ in the form of an interfacial reaction, without any loss of N in the remnant SiAlN coating.

As for the different thicknesses of SiAlN coatings, the above results obtained from this study have shown that identical SiAlN (Si_3N_4/AlN) coatings from a morphology and composition point of view, but with different layer thicknesses (0.4 µm, 0.8 µm, and 1.6 µm thick) display different performances upon exposure to the same thermal cycling conditions. The degradation of SiAlN coatings at different thicknesses follows the above discussed Scenario |||. The thinnest SiAlN coating needs a short period of thermal exposure to be depleted and the thickest SiAlN coating needs relatively long time to be fully depleted, as shown by schematic diagrams in Fig.12. Even if the reaction between Ti and SiAlN inevitably occurs, the reaction product, $TiN_{0.26}$, is mainly distributed between the substrate and SiAlN coating and is capable of serving as a diffusion barrier to mitigate further interaction between Ti and SiAlN. A thick SiAlN coating, i.e., $\geqslant$0.8 µm or 1.6 µm if in-service at 800°C, needs longer thermal exposure to deplete the SiAlN and also enables the formation of a certain thickness of $TiN_{0.26}$ layer, and therefore is desirable for a protective coating design. As for the role of the Mo interlayer, a thin

Mo layer is still desirable for a coating design as it could promote the integrity of a coating system without cracking or spallation via diffusion bonding and promoting the beneficial distribution of mechanical twinning. Neveretheless, it seems that the Mo interlayer has a negligible effect on the depletion of the SiAlN coating. After identical 20 h of exposure at 800°C , the 0.8 µm thick SiAlN coating without a Mo interlayer and the 0.8 µm thick SiAlN coating with a 0.3 µm thick Mo have the same thickness of residual SiAlN coating to a certain extent, as confirmed in Fig. 2 a and c, respectively.

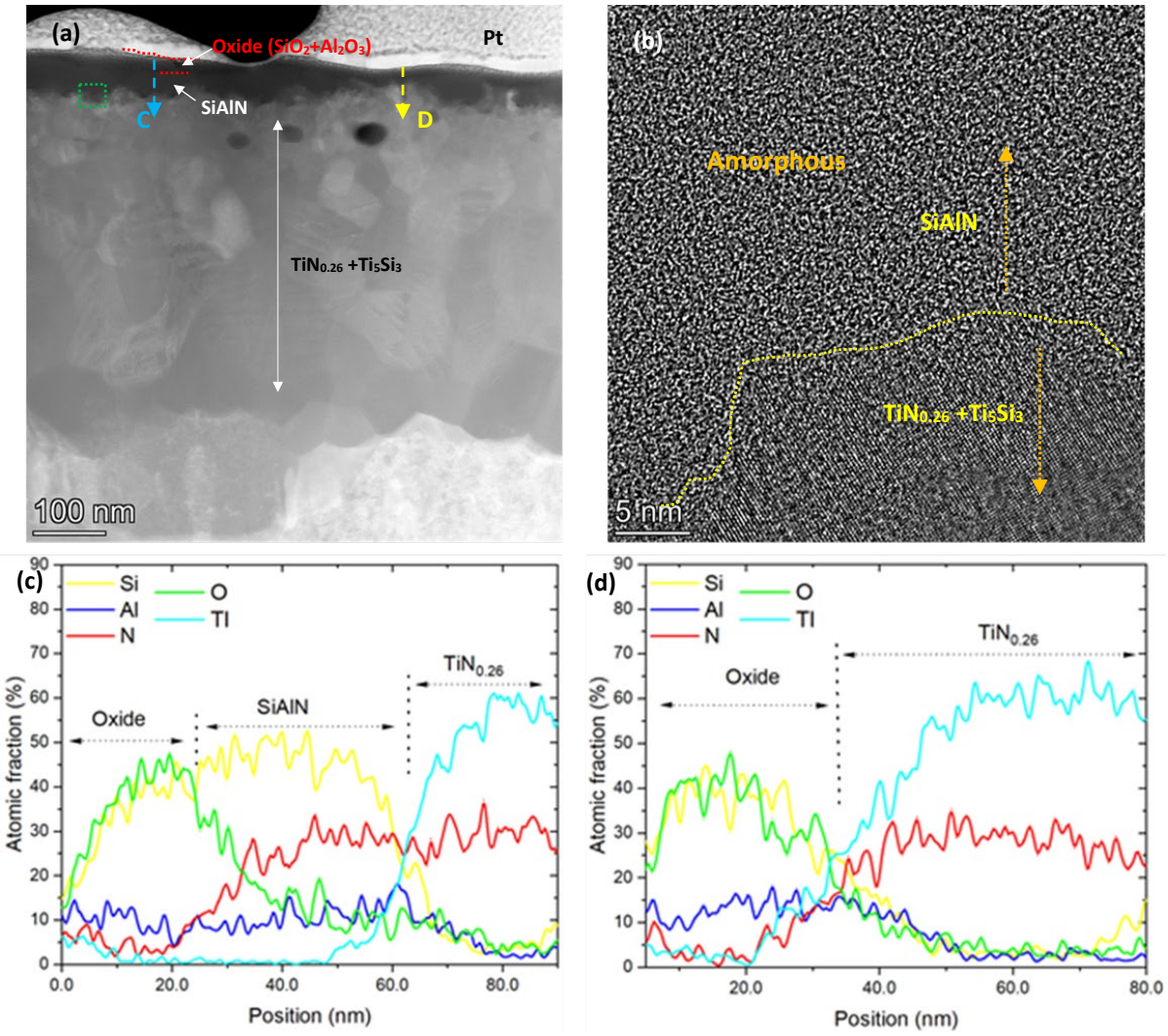

Fig.10 Cross-sectional HAADF/HRTEM micrographs and EDS line scans of SiAlN (0.4 µm thick) with Mo (0.3 µm) after oxidation at 800°C for 5 h (1 cycle): (a) HAADF image; (b) HRTEM micrograph, from the framed green region in (a); (c) EDS line scan along the blue line 'C' in (a), (d) EDS line scan along the yellow line 'D' in (a).

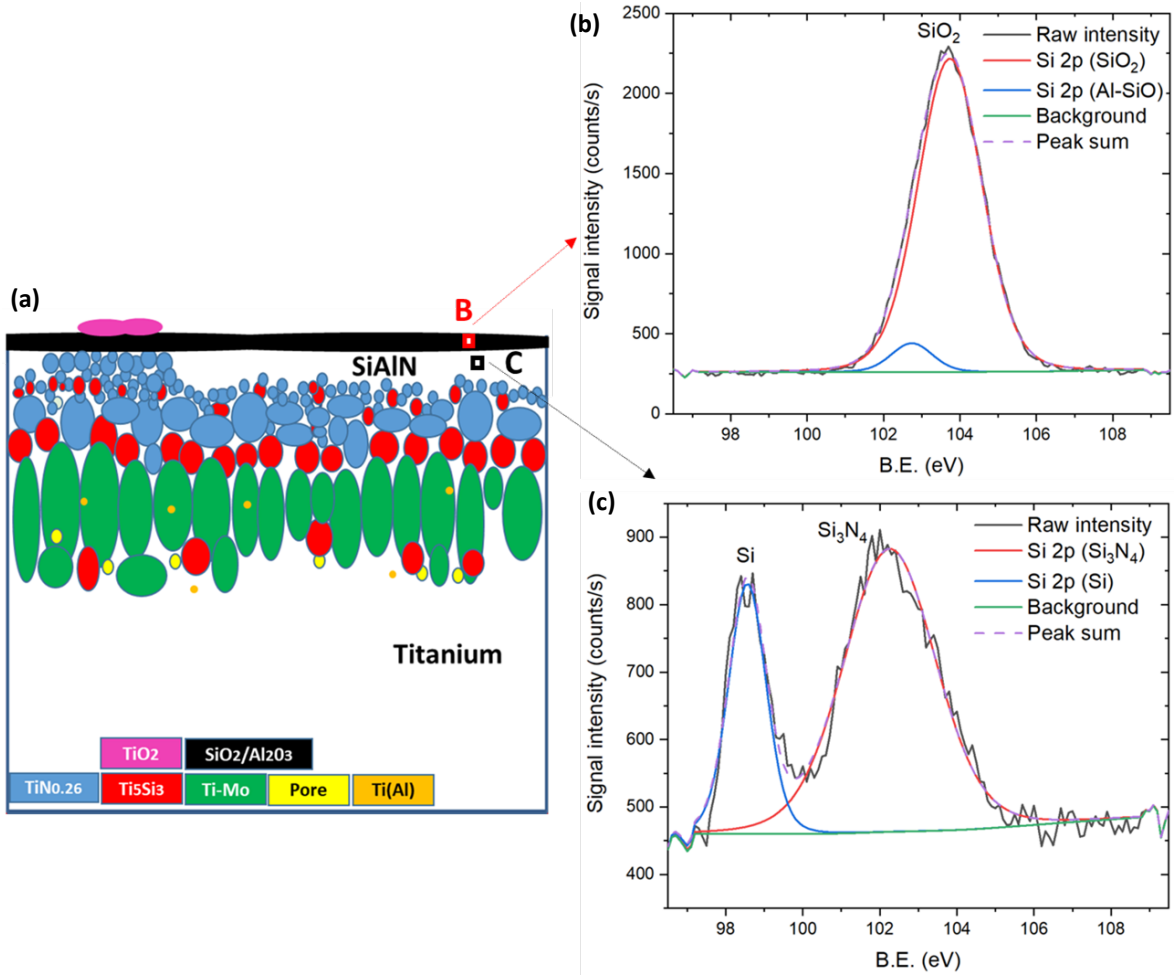

Fig. 11 FIB-XPS analysis on SiAlN (0.4 µm thick) with Mo (0.3 µm) after oxidation at 800°C for 5 h (1 cycle). (a) Schematic diagram of SiAlN coating with Mo after oxidation; (b) Si 2p XPS spectra of oxide, acquired from the position close to outermost surface of oxide, red rectangular box in (a); (c) Si 2p XPS spectra of remnant SiAlN, black rectangular box in (a); milling depth was validated.

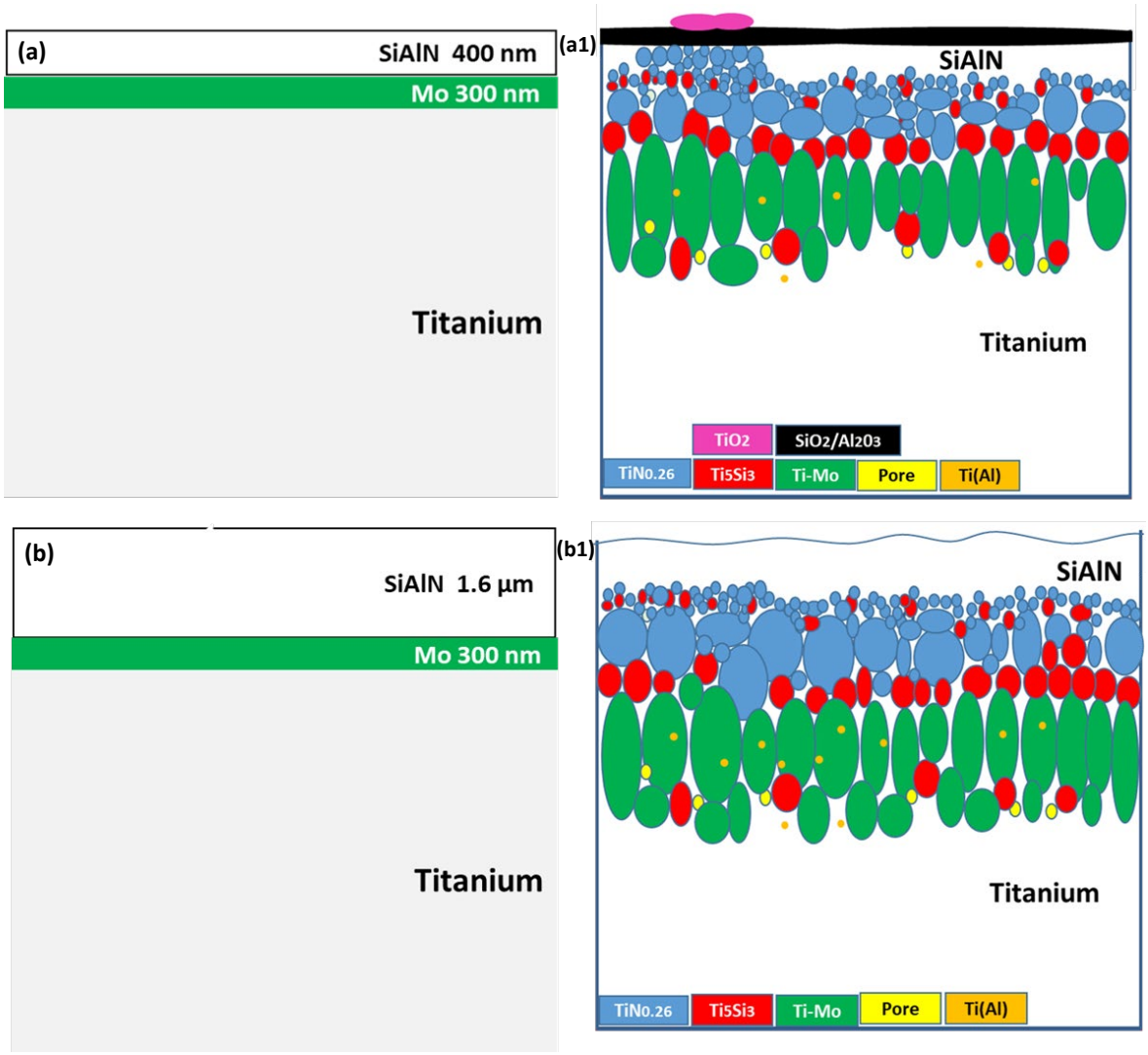

Fig.12 Schematic diagrams on degradation of SIAlN/Mo coatings after oxidation: (a) and (a1) As-deposited and thermal exposed SiAlN (0.4 µm thick) with Mo (0.3 µm), (a1) showing the existence of oxides; (b) and (b1) As-deposited and thermal exposed SiAlN (1.6 µm thick) with Mo (0.3 µm).

5. Conclusion

In conclusion, we have designed different amorphous SiAlN coatings having different thicknesses, with or without Mo interlayers on Ti substrates by magnetron sputtering. The 0.4 µm, 0.8 µm, and 1.6 µm thick SiAlN coatings with 0.3 µm Mo interlayers exhibit excellent cyclic oxidation protection at 800°C for 50 h (10 cycles). The degradation of the SiAlN/Mo coatings is determined by the depletion of the coatings induced by purely interfacial diffusion and reaction with the underlying Ti substrate. Once the remnant SiAlN coating is below a few tens of nanometers (i.e., almost fully depleted), the interfacial reaction causes a chemical change in the composition of the remnant amorphous SiAlN

coating, thereby causing oxidation of the remnant SiAlN coating. The prerequisite to maintaining the protective role of the coating is increasing the thickness of the SiAlN coating itself, as the interfacial diffusion/inter-reaction between the coating and the substrate occurs inevitably. The Mo interlayer can diffuse into the underlying Ti substrate and promote the formation of a continuous $TiN_{0.26}$ twining interlayer, thereby improving the interfacial performance in comparison with the coatings without Mo interlayers.

Acknowledgment

PX would like to acknowledge support from Royal Academy of Engineering and Rolls-Royce for the appointment of Rolls-Royce/Royal Academy of Engineering Research Chair in Advanced Coating Technology.

Reference

[1] T.S. Schmidt, S. Sewerin, Technology as a driver of climate and energy politics, Nat. Energy 2(6) (2017).

[2] M.G. Nitin P. Padture, Eric H. Jordan, Thermal barrier coatings for gas-turbine engine applications, Science 296 (2002) 280-284.

[3] G. Chen, Y. Peng, G. Zheng, Z. Qi, M. Wang, H. Yu, C. Dong, C.T. Liu, Polysynthetic twinned TiAl single crystals for high-temperature applications, Nat. Mater. 15(8) (2016) 876-81.

[4] D. Wei, P. Zhang, Z. Yao, J. Zhou, X. Wei, P. Zhou, A Cyclic oxidation behavior of plasma surface chromising coating on titanium alloy Ti–6Al–4V, Appl. Surf. Sci. 261 (2012) 800-806.

[5] D. Zhang, D. Qiu, M.A. Gibson, Y. Zheng, H.L. Fraser, D.H. StJohn, M.A. Easton, Additive manufacturing of ultrafine-grained high-strength titanium alloys, Nature 576(7785) (2019) 91-95.

[6] J.C. Williams, E.A. Starke, Progress in structural materials for aerospace systems11The Golden Jubilee Issue—Selected topics in Materials Science and Engineering: Past, Present and Future, edited by S. Suresh, Acta Mater. 51(19) (2003) 5775-5799.

[7] J.A. Hooker, P.J. Doorbar, Metal matrix composites for aeroengines, Mater. Sci. Technol. 16(7-8) (2013) 725-731.

[8] G.-H. Zhao, X. Xu, D. Dye, P.E.J. Rivera-Díaz-del-Castillo, Microstructural evolution and strain-hardening in TWIP Ti alloys, Acta Mater. 183 (2020) 155-164.

[9] Z. Shen, G. Liu, R. Zhang, J. Dai, L. He, R. Mu, Thermal property and failure behavior of LaSmZrO thermal barrier coatings by EB-PVD, iScience 25(4) (2022) 104106.

[10] Z. Shen, G. Liu, L. He, R. Mu, J. Dai, Thermal property and failure behaviors of Gd doped LaZrCeO coatings with feathery microstructure, npj Mater. Degrad. 6(1) (2022).

[11] Z. Shen, G. Liu, J. Dai, B. Huang, R. Mu, L. He, Thermal property and failure mechanism of LaDyZrO thermal barrier coatings by electron beam physical vapor deposition, Mater. Today Phys. 24 (2022).

[12] J. Dai, J. Zhu, C. Chen, F. Weng, High temperature oxidation behavior and research status of modifications on improving high temperature oxidation resistance of titanium alloys and titanium aluminides: A review, J. Alloys Compd. 685 (2016) 784-798.

[13] Z. Gao, Z. Zhang, X. Zhang, J. Kulczyk-Malecka, H. Liu, P. Kelly, P.J. Withers, P. Xiao, A conformable high temperature nitride coating for Ti alloys, Acta Mater. 189 (2020) 274-283.

[14] M. Zhang, Y. Cheng, L. Xin, J. Su, Y. Li, S. Zhu, F. Wang, Cyclic oxidation behaviour of Ti/TiAlN composite multilayer coatings deposited on titanium alloy, Corros. Sci. 166 (2020).

[15] L.-K. Wu, J.-J. Wu, W.-Y. Wu, F.-H. Cao, M.-Y. Jiang, Sol–gel-based coatings for oxidation protection of TiAl alloys, J. Mater. Sci. 55(15) (2020) 6330-6351.

[16] S. Leea, B. Sona, G. Parka, J. Ryua, H. Leeb, Investigation of short-term, high-temperature oxidation of AlCrN coating on WC substrate, Appl. Surf. Sci. 505 (2020) 144587.

[17] Y. Liao, B. Zhang, M. Chen, M. Feng, J. Wang, S. Zhu, F. Wang, Self-healing metal-enamel composite coating and its protection for TiAl alloy against oxidation under thermal shock in NaCl solution, Corros. Sci. 167 (2020).

[18] Y. Li, C. Chen, T. Han, J. Ranabhat, X. Feng, Y. Shen, Microstructures and oxidation behavior of NiCrAlCoY-Al composite coatings on Ti-6Al-4V alloy substrate via high-energy mechanical alloying method, J. Alloys Compd. 697 (2017) 268-281.

[19] S.P. Trivedi, D.K. Das, Microstructural aspects of plain aluminide and Pt-aluminide coatings on Ti-base alloy IMI-834, Intermetallics 13(10) (2005) 1122-1133.

[20] M. Mitoraj-Królikowska, E. Godlewska, Silicide coatings on Ti-6Al-1Mn (at.%) alloy and their oxidation resistance, Surf. Coat. Technol. 334 (2018) 491-499.

[21] Z.T. Wu, Z.B. Qi, B.B. Wei, D.F. Zhang, Z.C. Wang, Understanding hardness evolution of Zr–Si–N nanocomposite coatings via investigating their deformation behaviors, J. Eur. Ceram. Soc. 36(14) (2016) 3329-3339.

[22] L. Chavee, E. Serag, M. S. Pires, S. Lucas, E. Haye, A mechanistic approach of oxidation resistance, structural and mechanical behaviour of TiAlN coatings, Appl. Surf. Sci. 586 (2022) 152851.

[23] Z. Gao, J. Kulczyk-Malecka, Z. Zhang, H. Liu, X. Zhang, Y. Chen, P. Hill, P. Kelly, P. Xiao, Oxidation and degradation of amorphous SiAlN coating via forming Si-Si bond, Corros. Sci. 183 (2021).

[24] J. Musil, Hard nanocomposite coatings: Thermal stability, oxidation resistance and toughness, Surf. Coat. Technol. 207 (2012) 50-65.

[25] I. Gurrappa, A.K. Gogia, Development of oxidation resistant coatings for titanium alloys, Mater. Sci. Technol. 17(5) (2013) 581-587.

[26] X. Gong, R. Chen, Q. Wang, Y. Wang, N. Zhang, Z. Zhang, H. Fu, Cyclic oxidation behavior and oxide scale adhesion of Al/NiCrAlY coating on pure titanium alloy, J. Alloys Compd. 729 (2017) 679-687.

[27] W. Li, S. Zhu, M. Chen, C. Wang, F. Wang, Development of an oxidation resistant glass–ceramic composite coating on Ti–47Al–2Cr–2Nb alloy, Appl. Surf. Sci. 292 (2014) 583-590.

[28] Y. Zhao, M. Lu, Z. Fan, P. McCormick, Q. Tan, N. Mo, H. Huang, Microstructures and mechanical properties of wear-resistant titanium oxide coatings deposited on Ti-6Al-4V alloy using laser cladding, J. Eur. Ceram. Soc. 40(3) (2020) 798-810.

[29] W.W. Xu, S.L. Shang, B.C. Zhou, Y. Wang, L.J. Chen, C.P. Wang, X.J. Liu, Z.K. Liu, A first-principles study of the diffusion coefficients of alloying elements in dilute alpha-Ti alloys, Phys. Chem. Chem. Phys. 18(25) (2016) 16870-81.

[30] J.-W. Lu, Y.-Q. Zhao, P. Ge, H.-Z. Niu, Microstructure and beta grain growth behavior of Ti–Mo alloys solution treated, Mater. Charact. 84 (2013) 105-111.

[31] J. Musil, J. Vlček, P. Zeman, Hard amorphous nanocomposite coatings with oxidation resistance above 1000°C, Adv. Appl. Ceram. 107(3) (2013) 148-154.

[32] K.A. Kuptsov, P.V. Kiryukhantsev-Korneev, A.N. Sheveyko, D.V. Shtansky, Structural transformations in TiAlSiCN coatings in the temperature range 900–1600 °C, Acta Mater. 83 (2015) 408-418.

[33] S.H. Sheng, R.F. Zhang, S. Vepřek, Decomposition mechanism of Al1−xSixNy solid solution and possible mechanism of the formation of covalent nanocrystalline AlN/Si3N4 nanocomposites, Acta Mater. 61(11) (2013) 4226-4236.

[34] Y.S. Li, S. Shimada, H. Kiyono, A. Hirose, Synthesis of Ti–Al–Si–N nanocomposite films using liquid injection PECVD from alkoxide precursors, Acta Mater. 54(8) (2006) 2041-2048.

[35] I. Saladukhin, G. Abadias, V. Uglov, S. Zlotski, A. Janse van Vuuren, J. Herman O'Connell, Structural Properties and Oxidation Resistance of ZrN/SiNx, CrN/SiNx and AlN/SiNx Multilayered Films Deposited by Magnetron Sputtering Technique, Coatings 10(2) (2020).

[36] R. Daniel, J. Musil, P. Zeman, C. Mitterer, Thermal stability of magnetron sputtered Zr–Si–N films, Surf. Coat. Technol. 201(6) (2006) 3368-3376.

[37] P. Zeman, J. Musil, Difference in high-temperature oxidation resistance of amorphous Zr–Si–N and W–Si–N films with a high Si content, Appl. Surf. Sci. 252(23) (2006) 8319-8325.

[38] J. Musil, M. Šašek, P. Zeman, R. Čerstvý, D. Heřman, J.G. Han, V. Šatava, Properties of magnetron sputtered Al–Si–N thin films with a low and high Si content, Surf. Coat. Technol. 202(15) (2008) 3485-3493.

[39] K.E.S. R.E.T. Honghua Du, Carlo G. Pantano,, Oxidation studies of crystalline CVD silicon nitride, J. Electrochem. Soc. 136 (1989) 1527-1536.

[40] R.M. Horton, Oxidation kinetics of powdered silicon nitride, J. Am. Ceram. Soc. 52 (1968) 121-124.